Kinetics of Contraction-Induced GLUT4 Translocation in Skeletal Muscle Fibers From Living Mice

Hans P.M.M. Lauritzen,[1] Henrik Galbo,[2] Taro Toyoda,[1] and Laurie J. Goodyear[1]

OBJECTIVE—Exercise is an important strategy for the treatment of type 2 diabetes. This is due in part to an increase in glucose transport that occurs in the working skeletal muscles. Glucose transport is regulated by GLUT4 translocation in muscle, but the molecular machinery mediating this process is poorly understood. The purpose of this study was to *1*) use a novel imaging system to elucidate the kinetics of contraction-induced GLUT4 translocation in skeletal muscle and *2*) determine the function of AMP-activated protein kinase α2 (AMPKα2) in this process.

RESEARCH DESIGN AND METHODS—Confocal imaging was used to visualize GLUT4-enhanced green fluorescent protein (EGFP) in transfected quadriceps muscle fibers in living mice subjected to contractions or the AMPK-activator AICAR.

RESULTS—Contraction increased GLUT4-EGFP translocation from intracellular vesicle depots to both the sarcolemma and t-tubules with similar kinetics, although translocation was greater with contractions elicited by higher voltage. Re-internalization of GLUT4 did not begin until 10 min after contractions ceased and was not complete until 130 min after contractions. AICAR increased GLUT4-EGFP translocation to both sarcolemma and t-tubules with similar kinetics. Ablation of AMPKα2 activity in AMPKα2 inactive transgenic mice did not change GLUT4-EGFP′s basal localization, contraction-stimulated intracellular GLUT4-EGFP vesicle depletion, translocation, or re-internalization, but diminished AICAR-induced translocation.

CONCLUSIONS—We have developed a novel imaging system to study contraction-stimulated GLUT4 translocation in living mice. Contractions increase GLUT4 translocation to the sarcolemma and t-tubules with similar kinetics and do not require AMPKα2 activity. ***Diabetes*** **59:2134–2144, 2010**

Skeletal muscle is critical in the regulation of glucose homeostasis, being the major site of whole-body glucose disposal (1). In skeletal muscle fibers, the GLUT4 protein mediates increases in glucose uptake. Upon stimulation with insulin or muscle contraction, GLUT4 is translocated from intracellular vesicle compartments to the two main muscle membrane surfaces, the sarcolemma and t-tubules (2–5). The kinetics of GLUT4 intracellular trafficking in skeletal muscle and how signaling molecules regulate GLUT4 translocation are poorly understood, especially for contraction-mediated GLUT4 translocation. The majority of studies analyzing GLUT4 translocation dynamics have been carried out in adipocytes (6–10) or in muscle cell cultures (11–13), cell types that do not resemble fully differentiated muscle (14).

Recently, intravital imaging techniques have allowed detailed analysis of the spatial-temporal dynamics of GLUT4 translocation in response to insulin stimulation in skeletal muscle fibers of living animals (5,15,16). Direct imaging of insulin-stimulated GLUT4-EGFP translocation has shown that GLUT4 is translocated to both the sarcolemma and t-tubules. Both GLUT4 translocation and re-internalization were delayed in the t-tubules compared with the sarcolemma due to a lag in insulin diffusion (5,16). These imaging studies have also shown that in states of insulin resistance, the t-tubules, and not the sarcolemma, are the primary site of impaired insulin signaling and GLUT4 translocation (16). Collectively, these findings illustrate that insulin-mediated signaling and GLUT4 translocation are compartmentalized in mature skeletal muscle fibers.

It is unknown whether a similar type of compartmentalization exists for contraction-mediated GLUT4 translocation. It is well established that rapid spreading of membrane depolarization throughout the t-tubule network results in simultaneous activation of contraction throughout the muscle fiber (17).

Biochemical studies have suggested that in response to muscle contraction, GLUT4 can translocate to both the sarcolemma and t-tubules (4,18). However, imaging studies have never been done in intact contracting skeletal muscle to analyze the kinetics of GLUT4 translocation in high resolution.

The signaling mechanisms mediating contraction-induced GLUT4 translocation are not fully understood, but differ from those triggered by insulin (19). Muscle contractions increase AMPK activity (20), and pharmacological activation of AMPK results in increased glucose transport in skeletal muscle (20–22), although one report suggested that AICAR only caused GLUT4 translocation to the sarcolemma (23). Surprisingly, studies directly assessing the role of AMPK in contraction-mediated glucose transport using animal models with ablated AMPK activity have been ambiguous. Contraction-mediated glucose transport was not impaired in whole-body knockouts of the AMPKα1 or AMPKα2 catalytic subunits (24). In muscle-specific AMPKα2 inactive transgenic mice, contraction- or exercise-mediated glucose transport was either partially reduced (25,26) or unaffected (27,28), but the effects of AMPK activity on GLUT4 translocation kinetics are not known.

In the current study, we used intravital imaging to determine GLUT4 translocation kinetics in contracting skeletal muscle. To understand the intracellular signals

From the [1]Research Division, Joslin Diabetes Center and Harvard Medical School, Boston, Massachusetts; and the [2]Department of Rheumatology and Institute of Inflammation Research, Rigshospitalet, Copenhagen University Hospital, Copenhagen, Denmark.

Corresponding author: Laurie J. Goodyear, laurie.goodyear@joslin.harvard.edu.

Received 17 February 2010 and accepted 24 June 2010. Published ahead of print at http://diabetes.diabetesjournals.org on 9 July 2010. DOI: 10.2337/db10-0233.

that regulate this effect, we used muscle-specific AMPKα2 inactive transgenic mice (27). We found that contraction-stimulated GLUT4 translocation occurs at both the sarcolemma and t-tubules with similar kinetics. Our data demonstrate that contractions elicited by a higher voltage resulted in a higher degree of translocation, and that GLUT4 remains at the cell surface for up to 2 h after the cessation of contraction. Finally, our data show that contraction-stimulated GLUT4 translocation is AMPKα2-independent.

RESEARCH DESIGN AND METHODS

Protocols complied with the guidelines of the Institutional Animal Care and Use Committee of the Joslin Diabetes Center and the National Institutes of Health. Male Imprinting Control Region (ICR) mice (aged 7–10 weeks) (Taconic, Hudson, NY), AMPKα2 inactive transgenic mice on an FVB background, and matched controls were studied (27).

Plasmid and transfection procedures. The construction of GLUT4-EGFP has been described previously (16,29). Mice were transfected as previously described (14,29,30). Mice were briefly anesthetized with 90 mg/kg pentobarbital i.p., and the skin was opened to expose the quadriceps muscle to the bombardment of DNA/gold particles using the Helios gene gun system. Each muscle was shot twice with 200 psi pressure with 1 μg DNA/0.5 mg gold (0.6 μm gold particle size). After transfection, the skin was closed using sutures and the animals were allowed to recover.

Time-lapse microscopy. Five days after transfection, mice were anesthetized and mounted in dental cement (5,29). For contraction experiments, immediately prior to mounting the mice, microelectrodes were placed into the superficial muscle fiber layer near the groin and knee region of the quadriceps muscle, producing single twitch contractions only in the superficial layers of the quadriceps muscle fibers without losing imaging focus. Such stimulation activates muscle fibers via stimulation of the motor nerve fibers and motor endplates. Stimulation was not applied directly to the nerve because it resulted in either no visually detectable contractions or entire muscle belly contractions resulting in loss of optical focus during contraction.

For AICAR stimulation, the mouse was mounted, a catheter was placed in a tail vein, and a single confocal image was taken. This was followed by an additional 30-min stabilization period followed by another basal image ($t = 0$). There was no significant difference between the two basal images.

For the contraction protocol, immediately after the second basal image ($t = 0$), direct electrical stimulation to the muscle fibers was initiated. Two contraction treatments of different intensities were used: *1*) contractions elicited by lower voltage and the parameters were frequency 2 Hz, duration 60 milliseconds, voltage 0.1–0.9 V, consisting of three bouts of 10 min, separated by 90 s of rest and *2*) contractions elicited by higher voltage and the parameters were frequency 2 Hz, duration 60 milliseconds, voltage 1.1–3.0 V, consisting of three bouts of 5 min, separated by 90 s of rest. Both protocols elicited repeated single twitch contractions. Protocols were selected based on empirical observations of contraction force taken together with what was possible without losing optical focus of the imaged muscle fiber. We did not use an increasing contraction frequency because it made it very difficult to continually monitor fiber contraction. In our experience, the voltage field intensity generated by a higher voltage induced visually greater fiber contraction amplitude. This difference in contraction intensity is what we refer to as high- or low-voltage contractions throughout the study.

Contractions of the imaged fibers were continually monitored during the contraction periods through the oculars of the microscope, and voltage was adjusted to maintain force. Images were collected at the end of each contraction period and every 10-min post-contraction up to 130 min. The imaging of a high-voltage in situ contraction period is shown in supplementary video 1 (available online at http://diabetes.diabetesjournals.org/cgi/content/full/dc10-0233/DC1), illustrating that clear images are not obtainable when the fibers are contracting.

For AICAR stimulation, AICAR was given as an intravenous bolus injection (1 g/kg) through the tail vein, and images were collected every 10 min for 240 min. Images were collected with a 63×, 1.2 NA Zeiss C-Apochromat objective on a Zeiss-LSM-410 confocal microscope with ArKr-488 nanometer (nm) laser line for excitation of EGFP, while green emission light was collected between 500 and 530 nm using the standard fluorescein isothiocyanate filter. Sulforhodamine B images were collected as described (5).

Image analysis. The tagged image file format (TIFF) images obtained with the Zeiss confocal software were imported into Metamorf Software (version 6.1; Universal Imaging). Image stacks were created, and brightness and contrast were adjusted. Since it has previously been reported that GLUT4 translocation and re-internalization in muscle are products of endocytosis and exocytosis movements, we measured the net amount of GLUT4-EGFP at the various time points (31). The net amount of GLUT4-EGFP at membrane surfaces was quantified using Metamorf Software by drawing thin regions of interest (ROIs) at the sarcolemma and t-tubule regions, excluding vesicle structures, as previously described (5,15,16). Briefly, intracellular vesicle depots were quantified by measuring changes in gray value intensity in GLUT4-EGFP vesicles larger than ~2 μm in the visible fiber area inside an ROI covering both sarcolemma and t-tubules (Fig. 1*A*). The threshold and classifying settings in the Metamorf Software were used to discriminate depots above 2 μm in size from the background and emerging staining of sarcolemma and t-tubules. These Metamorf settings were also used to further discriminate between perinuclear and nonperinuclear GLUT4-EGFP depots. For sarcolemma, measurements from both sarcolemma edges of the confocal picture were averaged, the perinuclear areas were excluded, and measurements were normalized to the area of the sarcolemma ROI (Fig. 1*B*). For t-tubules, measurements from four randomly chosen areas were averaged (Fig. 1*B*). To compensate for variation in GLUT4-EGFP expression among fibers, the arbitrary units shown are the actual gray value of ROI fluorescence divided by ROI fluorescence value at $t = 0$ (f/f_0).

To verify the striated appearance and orientation of the t-tubules, we used sulforhodamine B, a water soluble dye that is not taken up by muscle fibers but will fill and stain the lumen of the t-tubules (32–34) (Fig. 1*C*). Sulforhodamine B was injected into the tail vein, and a confocal picture of quadriceps fibers was obtained 3 min later when the dye had fully loaded the t-tubules. Staining resulted in two very strong vertical florescent lines representing the capillaries and interstitial space near the sarcolemma and fine striated lines indicating the lumen of the t-tubules. The difference in the intensity of the sulforhodamine B staining is due to the much smaller diameter of the t-tubule lumen (~100 nm) compared with the flanking capillaries (~40 μm) and interstitial space. This striated pattern for t-tubules is consistent with previous findings (4,5,15,35).

Statistical analysis. Gray value means from ROIs were imported into Sigma plot 10.0. Values obtained at the end of the various contraction bouts (Fig. 1) and calculated areas under the curve (Fig. 5) were compared between groups by *t* test. Data are means ± SE, $^*P < 0.05$.

RESULTS

Contraction stimulates GLUT4-EGFP translocation to both the sarcolemma and t-tubules. In the basal state, GLUT4-EGFP was found in larger and smaller vesicle structures (Fig. 1*D* and *E*) ($t = 0$, diagonal arrow) and in the perinuclear region ($t = 0$, vertical arrow), as has been previously reported (4,5,16,29,36). There was no continuous presence at the sarcolemma (Fig. 1*D* and *E*) ($t = 0$, horizontal arrow) and no regular striated pattern throughout the fiber. Following basal imaging, the superficial fibers of the quadriceps were contracted with high or low voltage. In mice subjected to high voltage contractions, there was marked staining along the sarcolemma by the 5 min time point (Fig. 1*D*) ($t = 5$), quantified as a 60% increase above basal (Fig. 1*F*). A striated pattern emerged inside the muscle fibers by 5 min showing translocation to the t-tubules (Fig. 1*D*) ($t = 5$). Compared with the basal state, there was a 90% increase in t-tubule GLUT4-EGFP after 5 min of contraction (Fig. 1*G*). In parallel, there was a marked depletion of GLUT4-EGFP vesicles in intracellular GLUT4-EGFP vesicle depots, which also included the perinuclear region (Fig. 1*D* [$t = 5$] and *H*). Two additional 5-min contraction periods further increased GLUT4-EGFP staining of sarcolemma and t-tubules (>200% increase from basal) simultaneously with a further reduction in GLUT4-EGFP vesicle depots (70% decrease from basal) (Fig. 1*D* [$t = 10$, $t = 15$] and *H*). The depot depletion corresponded to a 75% maximal reduction in nonperinuclear depots and a 65% maximal reduction in perinuclear depots.

With contractions elicited by low voltage, there was a significant but modest GLUT4-EGFP translocation to the sarcolemma by 10 min, which appeared in the form of

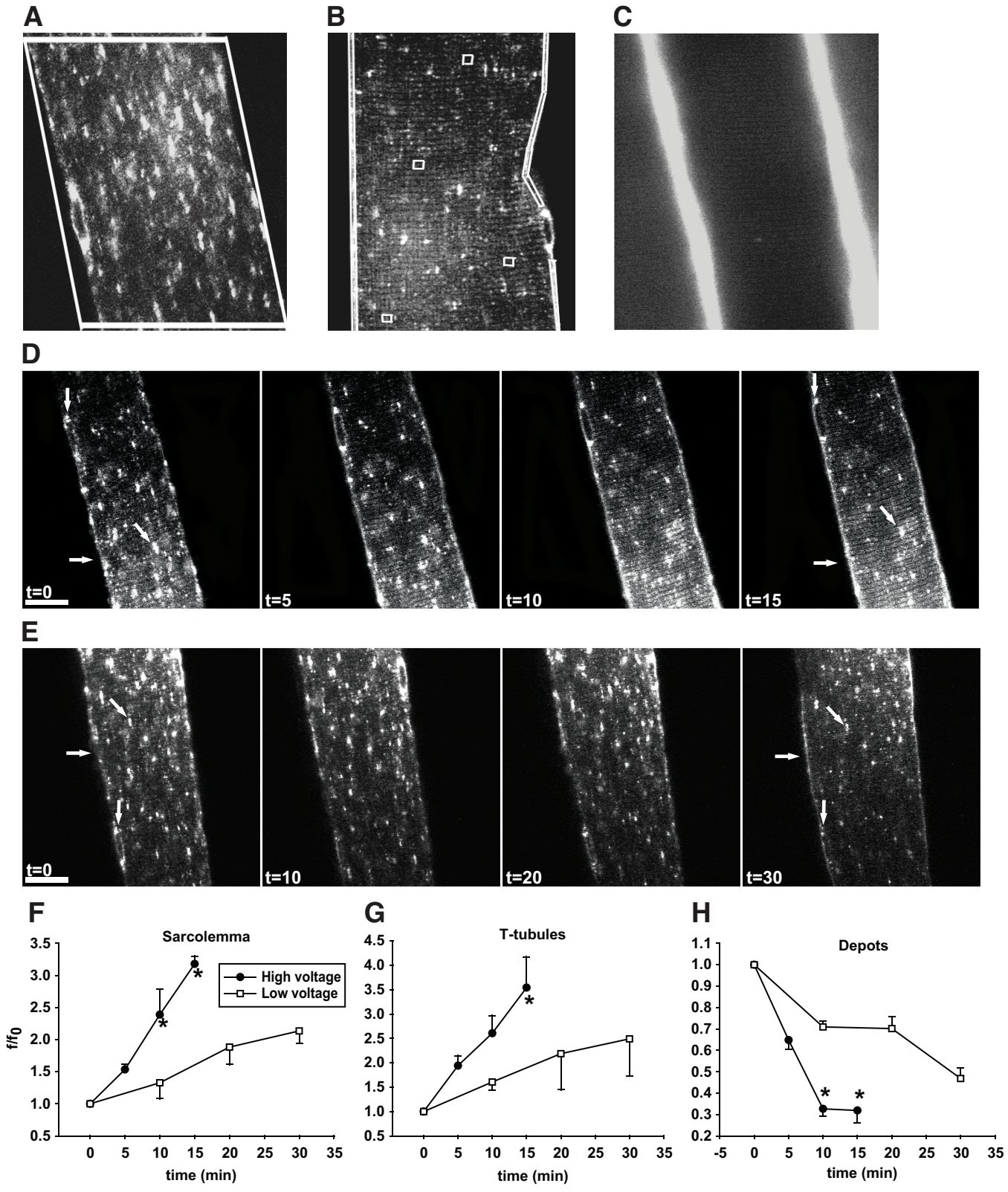

FIG. 1. Contraction-mediated GLUT4-EGFP translocation to both sarcolemma and t-tubules. *A* and *B*: Examples of the regions of interest (ROIs) used for image quantifications. *A*: Fluorescence values of GLUT4-EGFP perinuclear and nonperinuclear depots were measured within the same ROI. Quantification software settings were set to measure vesicles >2 μm in size inside the ROI and to discriminate between perinuclear and nonperinuclear depots. *B*: The level of GLUT4-EGFP translocation in the muscle fibers at the different time points was measured in ROIs along each sarcolemma side and in four randomly chosen ROIs in the t-tubules region. Translocation ROIs excluded vesicles structures above 2 μm in size. *C*: In vivo staining of t-tubules after intravenous injection of the water soluble dye sulforhodamine B, showing a high fluorescence staining in the capillaries running along the sarcolemma together with a more weakly fluorescent striated pattern in the t-tubules region. *D* and *E*: *t* =

continuous GLUT4-EGFP staining (Fig. 1*E* [$t = 10$] and *F*). There was also the emergence of t-tubule region striations (Fig. 1*E* [$t = 10$] and *G*). The increases in GLUT4-EGFP at the sarcolemma and t-tubules were accompanied by a 30% decrease in intracellular GLUT4 vesicle depots (Fig. 1*E* and *H*). During two additional 10-min periods of contractions, translocation to the sarcolemma and t-tubules steadily increased, and GLUT4-EGFP vesicle depots were further reduced (Fig. 1*E* [$t = 20$, $t = 30$, diagonal arrow] and *F–H*). Peak GLUT4-EGFP staining of the sarcolemma (Fig. 1*E*) ($t = 30$, horizontal arrow) and t-tubules (Fig. 1*E*) ($t = 30$, striated pattern) occurred at the same time, indicating that GLUT4 translocation to these distinct cell surface membranes followed similar kinetics (Fig. 1*F–H*). This is in contrast to what we have previously reported for insulin-mediated GLUT4-EGFP translocation (5). Comparison of high- and low-voltage contraction revealed that the high-voltage protocol resulted in greater levels of GLUT4-EGFP translocation to the sarcolemma and t-tubules and a greater decrease in GLUT4 vesicle depots (Fig. 1*F–H*).

Kinetics of GLUT4-EGFP re-internalization. We next investigated the kinetics of GLUT4-EGFP re-internalization in the period following muscle contractions, using the 3×5 min high-voltage contraction protocol that resulted in maximal translocation. Similar to the previous experiment (Fig. 1), GLUT4-EGFP translocation to the sarcolemma and t-tubules increased gradually throughout the contractions, and there was a concomitant decrease in intracellular depots (Fig. 2). Interestingly, peak GLUT4-EGFP depot depletion had occurred by 10 min (Fig. 2*A* [$t = 10$] and *D*), whereas GLUT4-EGFP translocation to the sarcolemma and t-tubules continued to increase during the first 10 min following the cessation of contractions (Fig. 2*A* [$t = +10$] and *B*,*C*). This indicates a delay in the arrival of GLUT4-EGFP at the sarcolemma and t-tubules. Following peak translocation to the sarcolemma and t-tubules, GLUT4-EGFP underwent gradual net re-internalization and was almost fully re-internalized by 130 min after contractions (Fig. 2*A–C*). In parallel, GLUT4-EGFP re-emerged in the depots (Fig. 2*A* and *D*). The time course of GLUT4-EGFP re-internalization was similar for the sarcolemma and t-tubules (Fig. 2*A–C*).

Contraction-stimulated GLUT4-EGFP translocation and re-internalization are normal in AMPKα2 inactive transgenic mice. AMPK has been proposed to regulate contraction-stimulated glucose transport in skeletal muscle, although there is now considerable data suggesting that AMPK is not necessary for this process (24,27,28). The role of AMPK in regulating GLUT4 translocation kinetics in skeletal muscle has not been studied. Here, contraction-regulated GLUT4-EGFP kinetics were compared in AMPKα2 inactive transgenic mice and their wild-type littermates. In the basal state, there was a normal distribution of GLUT4-EGFP in the intracellular depots and the perinuclear area (Fig. 3*A* and *B*) ($t = 0$, diagonal and vertical arrow), with no continuous presence at the sarcolemma and no regular continuous striated pattern (Fig. 3*A* and *B* [$t = 0$]). Thus, ablation of AMPKα2 activity did not affect GLUT4-EGFP localization in the basal state.

AMPKα2 inactive mice and their matched controls were subjected to 2×5 min of high-voltage stimulation. After contractions, GLUT4-EGFP was redistributed from the basal depots (Fig. 3*A*) ($t = 0$, $t = 10$, diagonal and vertical arrows) to the sarcolemma (Fig. 3*A*) ($t = 10$, horizontal arrow) and t-tubules (Fig. 3*A*) ($t = 10$, striated pattern). During 60 min of recovery, basal GLUT4-EGFP distribution was reestablished (Fig. 3*A*) ($t = 60$). When compared with controls, there was no difference in GLUT4-EGFP translocation and re-internalization (Fig. 3*B*). Image quantification showed that maximal translocation was reached at $t = 10$ min for both the sarcolemma (~260% above basal) (Fig. 3*C*) and t-tubules (~275% above basal) (Fig. 3*D*). This was accompanied by a 65% reduction in GLUT4-EGFP, corresponding to 65% maximal reduction in nonperinuclear depots and a 55% maximal reduction in perinuclear GLUT4-EGFP depots (Fig. 3*E*). Re-internalization of GLUT4-EGFP occurred immediately after contractions with similar rates for the sarcolemma and t-tubules indicating similar kinetics (Fig. 3*C* and *D*). Ablation of AMPKα2 activity did not influence GLUT4-EGFP kinetics in response to contractions (Fig. 3*C–E*). Thus, AMPKα2 activity is not necessary for normal GLUT4 trafficking kinetics before, during, and after in situ contractions in living animals.

AICAR-stimulated GLUT4-EGFP translocation and re-internalization. A previous study suggested that the AMPK activator AICAR only increases GLUT4 translocation to the sarcolemma and not to the t-tubules (23). However, this finding is not consistent with the central role of the t-tubules in GLUT4 translocation (4,5,35) and glucose transport (15,35) and the finding that AICAR stimulates glucose transport to the same extent as insulin and contraction (20). Therefore, we investigated the effects of AICAR on GLUT4-EGFP translocation kinetics. AICAR was injected as a bolus into the tail vein immediately after $t = 0$, and the first post-injection image was obtained 10 min later. AICAR resulted in a gradual but significant increase in staining along the sarcolemma by 20–40 min after AICAR injection (Fig. 4*A* [$t = 20–40$] and *B* [supplementary video 2]). Furthermore, a clear striated pattern appeared by 20–40 min after AICAR injection demonstrating GLUT4-EGFP translocation to the t-tubules (Fig. 4*A* [$t = 20–40$] and *C* [supplementary video 2]). Maximal translocation occurred 90–100 min after AICAR injection with a ~300% increase above basal for both the sarcolemma and t-tubules. Increased GLUT4-EGFP at the sarcolemma and t-tubules was accompanied by a gradual redistribution of GLUT4-EGFP from depots (Fig. 4). The depot depletion corresponded to a 70% maximal reduction in nonperinuclear depots and a 60% maximal reduction in perinuclear GLUT4-EGFP depots. GLUT4-EGFP vesicles were depleted 20 min after AICAR injection (Fig. 4) ($t = 20$, supplementary video 2), and depletion further progressed at 80 min (Fig. 4*D*). Re-internalization of GLUT4-

0 shows confocal images of basal GLUT4-EGFP–expressing ICR mouse muscle fibers just before in situ contractions. Repeated single contractions (2 Hz) were elicited using either "high" (1.1–3 V) (*D*) or "low" (0.1–0.9 V) (*E*) voltage. Muscle was stimulated for 3×5 min (*D*) or 3×10 min (*E*) periods separated by 90 sec of rest. Images are shown from one muscle fiber subjected to either high- (*D*) or low-voltage (*E*) contractions. Horizontal arrows indicate sarcolemma, while GLUT4-EGFP depots are indicated near the nuclei by vertical arrows and inside the fiber by diagonal arrows. Similar observations were done in fibers from five to eight mice. Numbers denote time in min. Bars = 20 μm. *F-H*: Image quantifications of GLUT4-EGFP at the sarcolemma (*F*), the t-tubules (*G*), and the intracellular vesicle depots (*H*). *Statistical difference between groups ($P < 0.05$) in values obtained at the end of identical contraction bouts. Arbitrary units shown are the actual grey value of ROI fluorescence divided by ROI fluorescence value at $t = 0$ (f/f_0). Data are means ± SE. $n = 5–8$.

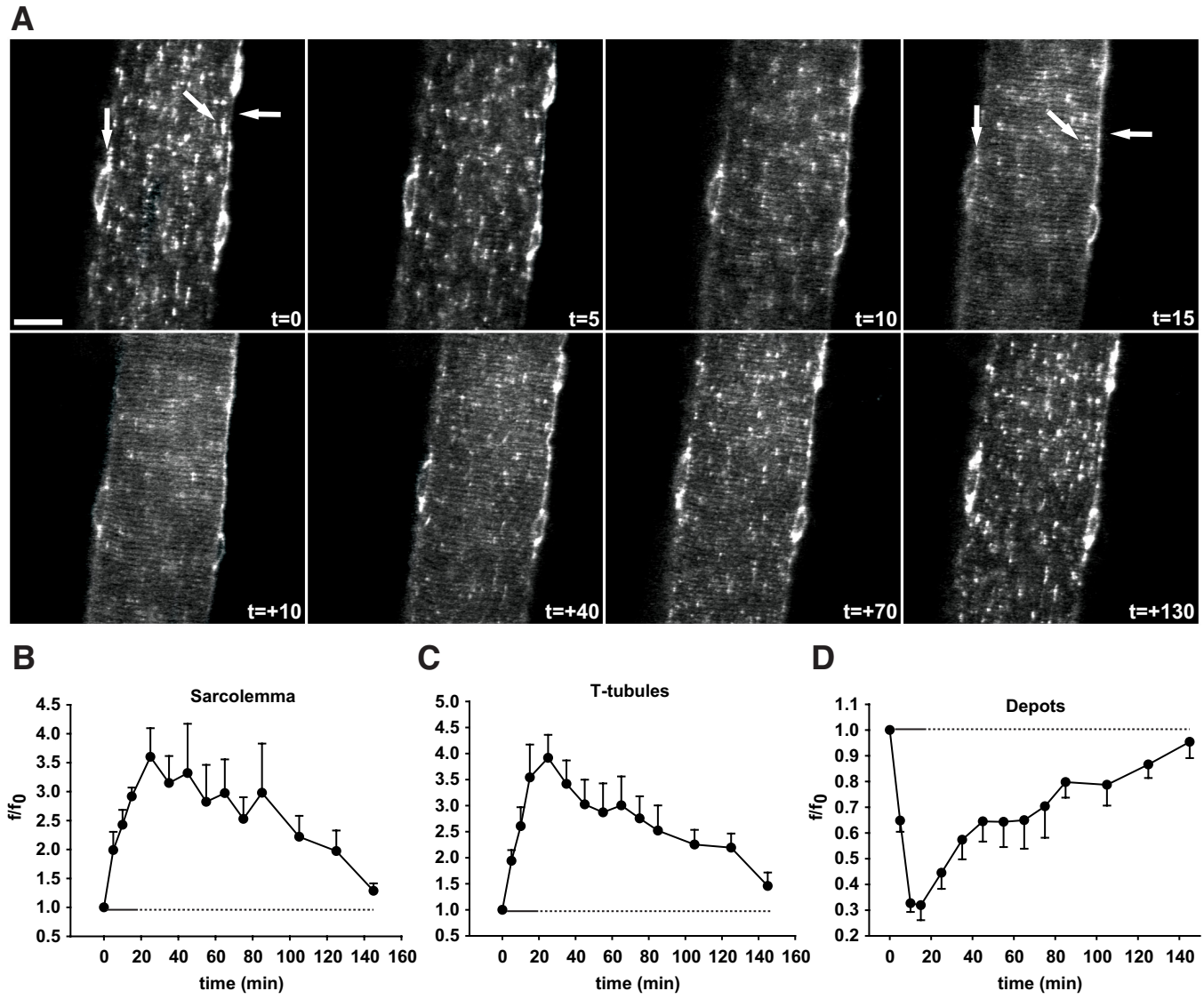

FIG. 2. In situ contractions induce GLUT4-EGFP translocation to and re-internalization from both sarcolemma and t-tubules with similar kinetics. *A*: *t*=0 shows confocal image of a basal GLUT4-EGFP–expressing muscle fiber just before in situ contractions in an ICR mouse. Contractions were elicited using the high-voltage protocol for 3 × 5 min separated by 90 sec of rest. Horizontal arrows indicate sarcolemma, while GLUT4-EGFP depots are indicated near the nuclei by vertical arrows and inside the fiber by diagonal arrows. Similar observations were done in fibers from five to eight mice. *t* = denotes accumulated contraction time; *t* = + denotes time during recovery after contractions. Bar = 20 μm. *B-D*: Image quantifications of GLUT4-EGFP at the sarcolemma (*B*), the t-tubules (*C*), and the intracellular vesicle depots (*D*). Horizontal solid lines indicate contraction period. Horizontal dotted lines indicate the period after contractions. Data are means ± SE. *n* = 5–8.

EGFP from the sarcolemma and t-tubules followed an identical time course (Fig. 4). Maximal translocation did not differ in response to AICAR (Fig. 4) and contractions (Figs. 1 and 2), and re-internalization kinetics were also similar in comparing the two stimuli (Figs. 1, 2, and 4). Thus, AICAR stimulates GLUT4-EGFP translocation to both the sarcolemma and t-tubules in a similar manner to muscle contraction.

AICAR-stimulated GLUT4-EGFP translocation is impaired in AMPKα2 inactive transgenic mice. We determined if AMPKα2 was necessary for AICAR-stimulated GLUT4-EGFP translocation. Compared with control mice, the AMPKα2 inactive transgenic mice had minor staining along the sarcolemma (Fig. 5*A* and *C*) and very weak striations in the t-tubule region following AICAR injection (Fig. 5*B* and *D*). Furthermore, there was only limited depletion of GLUT4-EGFP vesicle depots (Fig. 5*B* and *E*). It is interesting that the changes in the GLUT4-EGFP depots did not fully match sarcolemma and t-tubule GLUT4-EGFP, as there was a modest depletion of GLUT4-EGFP depots without an accompanying increase at the cell surface membranes (Fig. 5*C–E*). Based on our experience with this method, we believe that there is also an intermediate step in the GLUT4 translocation and re-internalization processes that appear as a light background "haze" upon imaging, and this haze can be observed in Fig. 5*A*.

The minimal GLUT4-EGFP translocation that is present in these mice may be due to very low levels of AMPKα1 subunit in the muscle fibers and/or from nonspecific systemic effects of AICAR. In fact, we observed that injection of AICAR caused minor trembling of the mice (this can be seen as the muscle fiber vibrating in first half of supplementary video 2). Thus, the majority of the AICAR-induced GLUT4-EGFP translocation is abolished in AMPKα2 inactive transgenic mice.

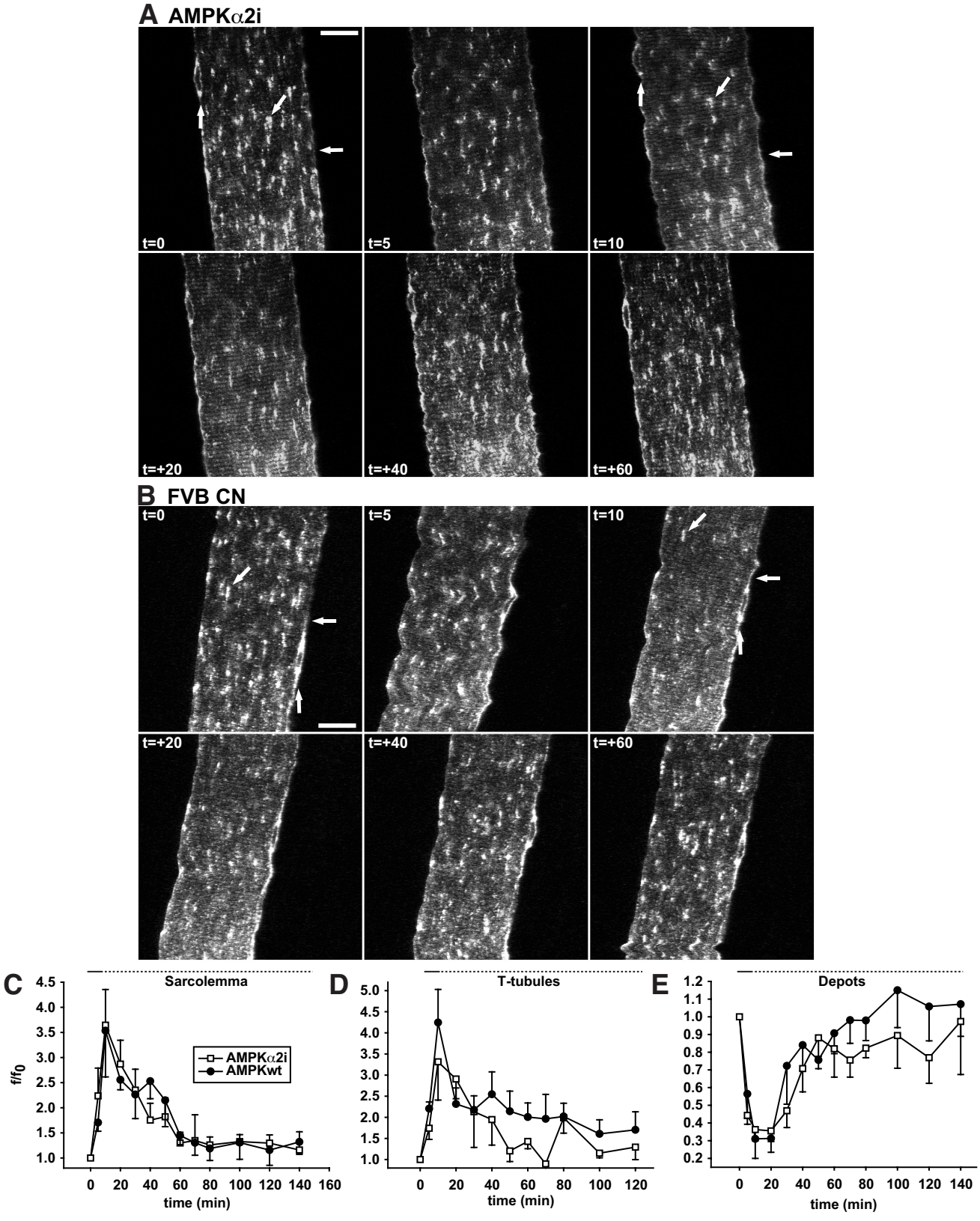

FIG. 3. AMPK activity does not affect GLUT4-EGFP basal localization and translocation and re-internalization kinetics in response to in situ contractions. *A* and *B*: $t = 0$ shows confocal images of basal GLUT4-EGFP–expressing muscle fibers immediately before in situ contractions in either a muscle-specific AMPKα2 inactive transgenic mouse (*A*) or a matched control mouse (*B*). Contractions were elicited using the high-voltage protocol for 2 × 5 min separated by 90 sec of rest. Horizontal arrows indicate sarcolemma, while GLUT4-EGFP depots are indicated near the nuclei by vertical arrows and inside the fibers by diagonal arrows. Similar observations were made in fibers from five mice in each group. Numbers denote time in min during ($t =$) and after ($t = +$) contractions. Bars = 20 μm. *C–E*: Image quantifications of GLUT4-EGFP at the sarcolemma (*C*), the t-tubules (*D*), and the intracellular vesicle depots (*E*). Horizontal solid lines indicate contraction period. Horizontal dotted lines indicate the period after contractions. Data are means ± SE. $n = 5$.

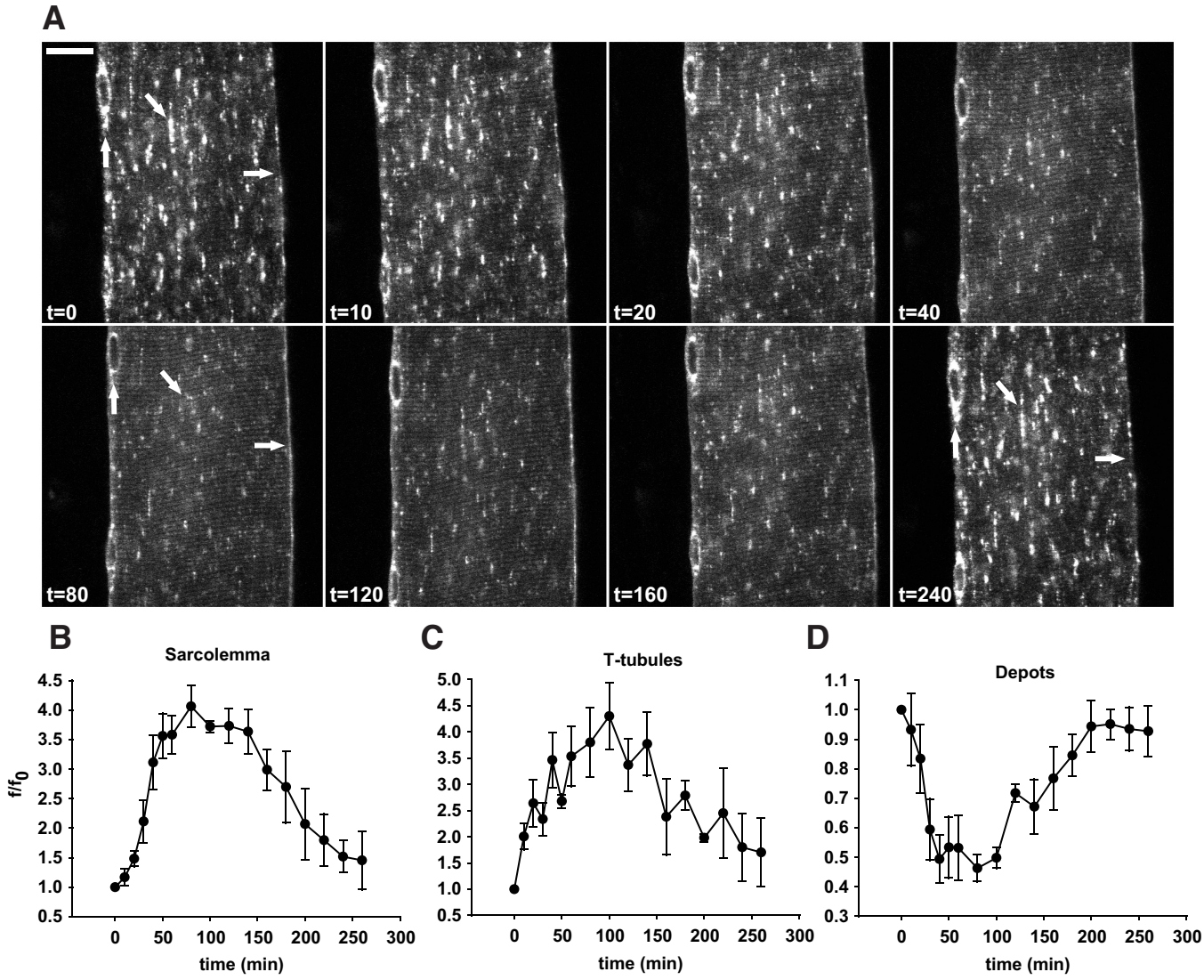

FIG. 4. AICAR stimulation induces GLUT4-EGFP translocation to both sarcolemma and t-tubules with similar kinetics. *A*: $t = 0$ shows a confocal image of a basal GLUT4-EGFP–expressing muscle fiber in situ immediately prior to intravenous AICAR administration via the tail vein of an anesthetized ICR mouse. Horizontal arrows indicate sarcolemma, while GLUT4-EGFP depots are indicated near the nuclei by vertical arrows and inside the fiber by diagonal arrows. Similar observations were made in fibers from five mice. Numbers denote time in min. Bar = 20 μm. *B–D*: Image quantifications of GLUT4-EGFP at the sarcolemma (*B*), the t-tubules (*C*), and the intracellular vesicle depots (*D*). Data are means ± SE. $n = 5$.

DISCUSSION

Physical exercise is accepted as an important modality to decrease blood glucose concentrations in patients with diabetes. Despite the importance of exercise in the maintenance of overall glucose homeostasis, the cellular machinery that controls contraction-stimulated glucose transport is poorly understood. In the current study, we used a newly developed imaging technique to investigate GLUT4 translocation by directly monitoring the kinetics of intramuscular GLUT4-EGFP translocation before, during, and after contraction of skeletal muscle fibers in living mice. We found that contraction increases GLUT4 translocation to both sarcolemma and t-tubules, this effect is voltage dependent, and GLUT4 on the cell surface membranes is increased for more than 2 h after the cessation of contraction. In examining a putative signaling mechanism, we found that AMPKα2 activity is not necessary for contraction-stimulated GLUT4 translocation.

Translocation to the sarcolemma and t-tubules, as well as depletion of intracellular vesicle depots, was higher in response to contractions elicited by higher voltage despite a 50% shorter duration of contraction compared with the low-voltage protocol. In addition, the high-voltage protocol resulted in a continuous increase in GLUT4-EGFP translocation to the sarcolemma and t-tubules for the 15-min period even though maximal intracellular GLUT4-EGFP vesicle depletion had occurred by 10 min (Fig. 1). The mechanism for the delay is not known; however, it could be the result of the ability of high-voltage contraction to accelerate depletion of GLUT4-EGFP storage vesicles rapidly, combined with a potential "bottleneck" at the exocytic/fusion step at the cell surface membranes. Such a bottleneck at the fusion step of GLUT4-EGFP translocation has previously been shown to occur in primary adipocytes (10). The magnitude of the increase in GLUT4-EGFP translocation was similar to that observed with myc-tagged-GLUT4 in

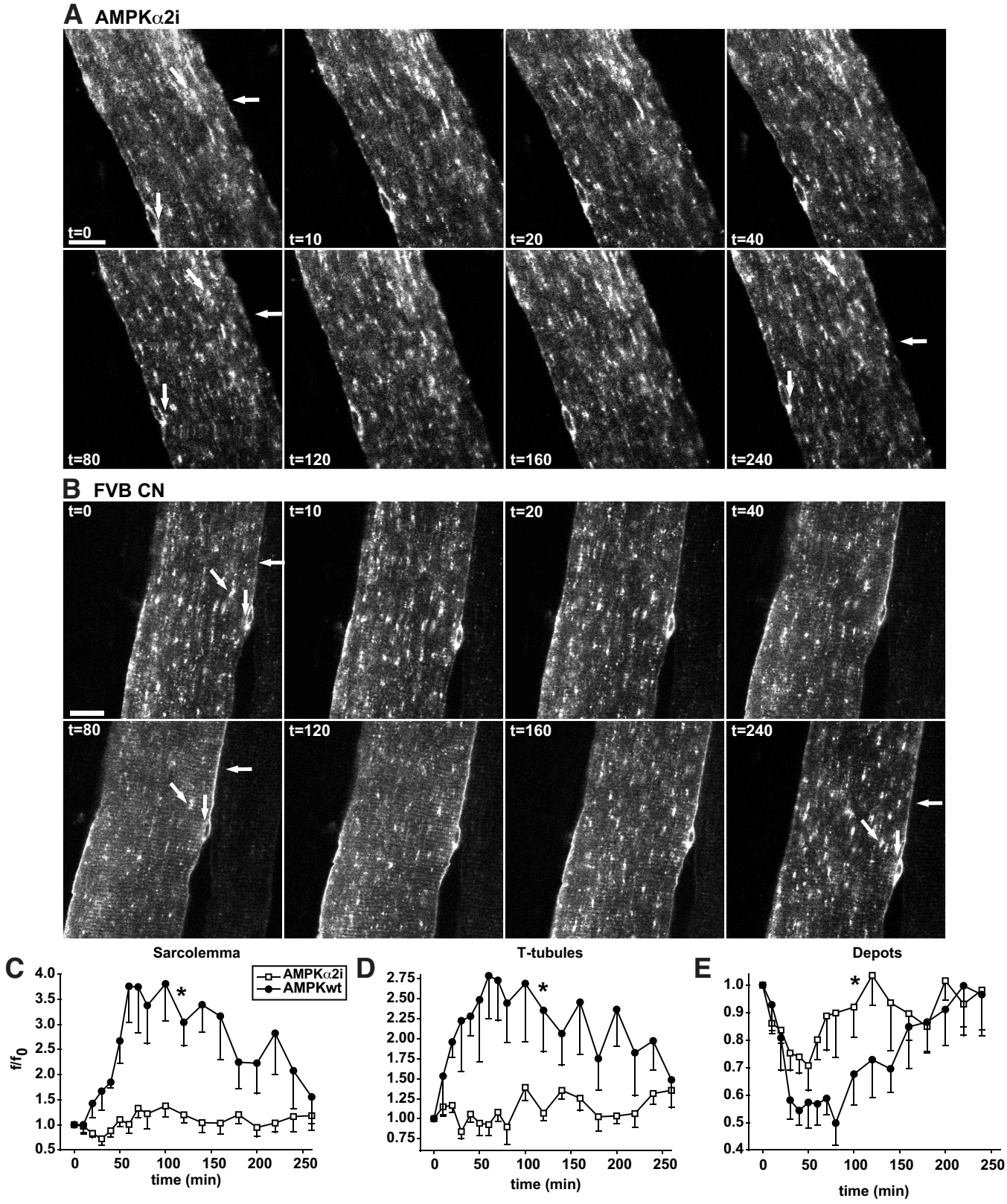

FIG. 5. Depletion of AMPKα2 activity markedly reduces AICAR-mediated GLUT4-EGFP translocation to both the sarcolemma and t-tubules. *A* and *B*: $t = 0$ shows confocal images of a basal GLUT4-EGFP–expressing muscle fiber in situ in either an AMPKα2 inactive transgenic mouse (*A*) or a matched control FVB mouse (*B*). Immediately after $t = 0$, AICAR was administrated intravenously via the tail vein. Horizontal arrows indicate sarcolemma, while GLUT4-EGFP depots are indicated near the nuclei by vertical arrows and inside the fiber by diagonal arrows. Similar observations were made in fibers from five to six mice in each group. Numbers denote time in min. Bars = 20 μm. *C–E*: Image quantifications of GLUT4-EGFP at the sarcolemma (*C*), the t-tubules (*D*), and the intracellular vesicle depots (*E*). Area under curves were calculated. *Statistical difference between groups ($P < 0.05$). Data are means ± SE. $n = 5–6$.

sarcolemmal giant vesicles fractionated from contracted mouse muscle (37) and collagenase-derived cardiomyocytes (38), although neither of these studies were performed in live animals.

Current theory suggests that excitation-contraction coupling in the individual muscle fiber occurs as an all or nothing event (17), and therefore an increase in stimulation above a threshold level would not have an additional effect on that muscle fiber. In contrast, our observations, which followed GLUT4 translocation throughout the entire contraction treatment in the same muscle fibers, indicate that voltage-dependent regulatory mechanisms exist within individual fibers. Thus, metabolically derived signals may control the magnitude and duration of contraction-stimulated GLUT4 translocation as opposed to mechanically derived stimulation.

It is well established that there are distinct signaling mechanisms for exercise- and insulin-stimulated glucose transport, due in part to data demonstrating that the combination of a maximal insulin stimulus plus a maximal contraction stimulus has additive effects on glucose transport (19,39) and GLUT4 translocation (4). Some studies suggest there are different intracellular pools of GLUT4, one stimulated by insulin and one stimulated by exercise (18,40,41). Although the current data do not directly support the possibility of different pools of GLUT4 in muscle, they do demonstrate that the spatial temporal kinetics of contraction- and insulin-stimulated GLUT4 translocation differ substantially. In a previous investigation, we analyzed recruitment, translocation, steady-state recycling, and subsequent re-internalization of GLUT4 in response to insulin in live mice. With insulin stimulation, we found GLUT4-EGFP translocation to the sarcolemma to be faster than GLUT4-EGFP translocation in the t-tubules. The delay was found to originate from a difference in initiation of the insulin signal. In parallel, GLUT4-EGFP re-internalization was also completed earlier at the sarcolemma compared with the t-tubules. In contrast, in the present study, we found that the kinetics of contraction-stimulated GLUT4 translocation and re-internalization to and from the sarcolemma and t-tubules are similar for the two compartments. These differences in GLUT4 translocation kinetics provide further evidence that the insulin- and contraction-stimulated translocation mechanisms for GLUT4 are distinct. One of the reasons for this difference could be that the contraction impulses spread rapidly at a similar rate throughout the cell to both the t-tubules and sarcolemma during excitation-contraction coupling. In contrast, insulin stimulation is initiated as insulin arrives first at the sarcolemma and, in turn, slowly diffuses into the t-tubules (5). Another possible reason could be that the signaling/translocation cascade differs between the sarcolemma and t-tubules for insulin stimulation, whereas the contraction cascade does not.

In addition to contraction and insulin, there are many other stimuli that increase glucose transport in skeletal muscle (20). The AMPK activator AICAR increases glucose transport and, through the use of subcellular fractionation, we (36) and another group (23) have shown that AICAR increases GLUT4 translocation. A more recent report (42) utilized a photolabeling technique and showed that AICAR increased GLUT4 translocation to the membrane fraction of rat muscle strips to the same extent as a supraphysiological insulin dose. Surprisingly, in another report (23), AICAR was shown to only stimulate GLUT4 translocation to the sarcolemmal membranes and not to the t-tubules. In the current investigation, AICAR clearly resulted in GLUT4 translocation to both the sarcolemma and t-tubules, and this redistribution of GLUT4 to the two membrane compartments adhered to similar kinetics. The discrepancy may be due to very different experimental techniques with subcellular fractionation methods that are less sensitive. Given our current findings, the fact that AICAR has robust effects on glucose transport and that detubulation experiments indicate a predominant role of t-tubules in regulating glucose transport in muscle (15,35), we believe t-tubules play a significant role in the regulation of AICAR-stimulated glucose transport.

AMPK activation has been proposed to be the key regulator of contraction-stimulated GLUT4 translocation (43), and AMPK activation by AICAR has been shown to increase glucose transport in skeletal muscle to the same extent as contractions (27). Consistent with these findings, we observed that AICAR and contractions resulted in similar increases in GLUT4 translocation in muscle fibers. To determine the role of AMPKα2 in AICAR- and contraction-stimulated GLUT4 localization and trafficking, we studied AMPKα2 inactive transgenic mice. AICAR-stimulated GLUT4-EGFP translocation was markedly reduced in the AMPKα2 inactive mice, consistent with previous results measuring abolished glucose transport (25,27). Interestingly, contraction-stimulated GLUT4 translocation and re-internalization kinetics for both the sarcolemma and t-tubules were identical in mice with ablated AMPKα2 activity. This is in line with a report that used subcellular fractionation to show that exercise in AMPKα2 kinase dead transgenic mice results in normal GLUT4 translocation (28). Our GLUT4 translocation findings are consistent with studies showing only partial (25) or no (27) inhibition of glucose transport in models of ablated AMPKα2. Thus, either AMPK is not involved in contraction-induced GLUT4 translocation or redundant mechanisms mediate signaling to the intracellular GLUT4 vesicle depots. Interestingly, ablation of AMPKα2 activity had no effect on basal distribution of GLUT4.

In summary, this study determined the effects of contraction on GLUT4 translocation and re-internalization kinetics directly in the skeletal muscle of living mice. To describe GLUT4 translocation with muscle contraction, we and other groups have previously used a laborious subcellular fractionation methodology (44,45). This early work demonstrated that both insulin and exercise increase glucose uptake via GLUT4 translocation from an intracellular pool to the plasma membrane. However, the novel microscopy technique described here has allowed us to significantly advance this line of investigation. By monitoring the localization and movement of fluorescent-labeled GLUT4 by confocal microscopy in the muscle fibers of anesthetized mice, we can observe the spatial-temporal details of GLUT4 localization and translocation. Previously, this level of quality and resolution of imaging was only possible in cell culture systems. In future studies, this method can be used to address important questions concerning contraction-induced GLUT4 translocation, such as how the GLUT4 vesicles interact with other proteins of the translocation machinery and the signals regulating GLUT4 translocation.

ACKNOWLEDGMENTS

This project was supported by grants from the National Institutes of Health (R01AR45670 and R01DK68626) (L.J.G.) and the Diabetes and Endocrinology Research Center at the Joslin Diabetes Center (P30DK036836). H.P.M.M.L. was supported by the Weimann Foundation, the Beckett Foundation, and the Danish National Research Foundation. T.T. was supported by an American Diabetes Association mentor-based fellowship (L.J.G.).

No potential conflicts of interest relevant to this article were reported.

H.P.M.M.L. designed and performed the experiments and wrote the manuscript. H.G. contributed to the discussion and reviewed and edited the manuscript. T.T. performed the experiments and contributed to the discussion. L.J.G. designed the experiments and wrote and edited the manuscript.

REFERENCES

1. Ferrannini E, Smith JD, Cobelli C, Toffolo G, Pilo A, DeFronzo RA. Effect of insulin on the distribution and disposition of glucose in man. J Clin Invest 1985;76:357–364
2. Wilson CM, Cushman SW. Insulin stimulation of glucose transport activity in rat skeletal muscle: increase in cell surface GLUT4 as assessed by photolabelling. Biochem J 1994;299:755–759
3. Marette A, Burdett E, Douen A, Vranic M, Klip A. Insulin induces the translocation of GLUT4 from a unique intracellular organelle to transverse tubules in rat skeletal muscle. Diabetes 1992;41:1562–1569
4. Ploug T, van Deurs B, Ai H, Cushman SW, Ralston E. Analysis of GLUT4 distribution in whole skeletal muscle fibers: identification of distinct storage compartments that are recruited by insulin and muscle contractions. J Cell Biol 1998;142:1429–1446
5. Lauritzen HP, Ploug T, Prats C, Tavaré JM, Galbo H. Imaging of insulin signaling in skeletal muscle of living mice shows major role of t-tubules. Diabetes 2006;55:1300–1306
6. Dobson SP, Livingstone C, Gould GW, Tavaré JM. Dynamics of insulin-stimulated translocation of GLUT4 in single living cells visualised using green fluorescent protein. FEBS Lett 1996;393:179–184
7. Oatey PB, Van Weering DH, Dobson SP, Gould GW, Tavaré JM. GLUT4 vesicle dynamics in living 3T3 L1 adipocytes visualized with green-fluorescent protein. Biochem J 1997;327:637–642
8. Oatey PB, Venkateswarlu K, Williams AG, Fletcher LM, Foulstone EJ, Cullen PJ, Tavaré JM. Confocal imaging of the subcellular distribution of phosphatidylinositol 3,4,5-trisphosphate in insulin- and PDGF-stimulated 3T3–L1 adipocytes. Biochem J 1999;344:511–518
9. Fletcher LM, Welsh GI, Oatey PB, Tavaré JM. Role for the microtubule cytoskeleton in GLUT4 vesicle trafficking and in the regulation of insulin-stimulated glucose uptake. Biochem J 2000;352:267–276
10. Lizunov VA, Matsumoto H, Zimmerberg J, Cushman SW, Frolov VA. Insulin stimulates the halting, tethering, and fusion of mobile GLUT4 vesicles in rat adipose cells. J Cell Biol 2005;169:481–489
11. Tong P, Khayat ZA, Huang C, Patel N, Ueyama A, Klip A. Insulin-induced cortical actin remodeling promotes GLUT4 insertion at muscle cell membrane ruffles. J Clin Invest 2001;108:371–381
12. Huang C, Somwar R, Patel N, Niu W, Török D, Klip A. Sustained exposure of L6 myotubes to high glucose and insulin decreases insulin-stimulated GLUT4 translocation but upregulates GLUT4 activity. Diabetes 2002;51:2090–2098
13. Fecchi K, Volonte D, Hezel MP, Schmeck K, Galbiati F. Spatial and temporal regulation of GLUT4 translocation by flotillin-1 and caveolin-3 in skeletal muscle cells. FASEB J 2006;20:705–707
14. Lauritzen HP, Schertzer JD. Measuring GLUT4 translocation in mature muscle fibers. Am J Physiol Endocrinol Metab 2010;299:E169–E179
15. Lauritzen HP, Ploug T, Ai H, Donsmark M, Prats C, Galbo H. Denervation and high-fat diet reduce insulin signaling in t-tubules in skeletal muscle of living mice. Diabetes 2008;57:13–23
16. Lauritzen HP, Galbo H, Brandauer J, Goodyear LJ, Ploug T. Large GLUT4 vesicles are stationary while locally and reversibly depleted during transient insulin stimulation of skeletal muscle of living mice: imaging analysis of GLUT4-enhanced green fluorescent protein vesicle dynamics. Diabetes 2008;57:315–324
17. Adrian E.D. The all-or-nothing reaction. Rev Physiol Biochem Pharmacol 1935;35:744–755
18. Roy D, Marette A. Exercise induces the translocation of GLUT4 to transverse tubules from an intracellular pool in rat skeletal muscle. Biochem Biophys Res Commun 1996;223:147–152
19. Goodyear LJ, Kahn BB. Exercise, glucose transport, and insulin sensitivity. Annu Rev Med 1998;49:235–261
20. Hayashi T, Hirshman MF, Kurth EJ, Winder WW, Goodyear LJ. Evidence for 5′ AMP-activated protein kinase mediation of the effect of muscle contraction on glucose transport. Diabetes 1998;47:1369–1373
21. Merrill GF, Kurth EJ, Hardie DG, Winder WW. AICA riboside increases AMP-activated protein kinase, fatty acid oxidation, and glucose uptake in rat muscle. Am J Physiol 1997;273:E1107–E1112
22. Ihlemann J, Ploug T, Hellsten Y, Galbo H. Effect of stimulation frequency on contraction-induced glucose transport in rat skeletal muscle. Am J Physiol Endocrinol Metab 2000;279:E862–E867
23. Lemieux K, Konrad D, Klip A, Marette A. The AMP-activated protein kinase activator AICAR does not induce GLUT4 translocation to transverse tubules but stimulates glucose uptake and p38 mitogen-activated protein kinases alpha and beta in skeletal muscle. FASEB J 2003;17:1658–1665
24. Jørgensen SB, Viollet B, Andreelli F, Frøsig C, Birk JB, Schjerling P, Vaulont S, Richter EA, Wojtaszewski JF. Knockout of the alpha2 but not alpha1 5′-AMP-activated protein kinase isoform abolishes 5-aminoimidazole-4-carboxamide-1-beta-4-ribofuranoside but not contraction-induced glucose uptake in skeletal muscle. J Biol Chem 2004;279:1070–1079
25. Mu J, Brozinick JT Jr, Valladares O, Bucan M, Birnbaum MJ. A role for AMP-activated protein kinase in contraction- and hypoxia-regulated glucose transport in skeletal muscle. Mol Cell 2001;7:1085–1094
26. Lee-Young RS, Griffee SR, Lynes SE, Bracy DP, Ayala JE, McGuinness OP, Wasserman DH. Skeletal muscle AMP-activated protein kinase is essential for the metabolic response to exercise in vivo. J Biol Chem 2009;284:23925–23934
27. Fujii N, Hirshman MF, Kane EM, Ho RC, Peter LE, Seifert MM, Goodyear LJ. AMP-activated protein kinase alpha2 activity is not essential for contraction- and hyperosmolarity-induced glucose transport in skeletal muscle. J Biol Chem 2005;280:39033–39041
28. Maarbjerg SJ, Jorgensen SB, Rose AJ, Jeppesen J, Jensen TE, Treebak JT, Birk JB, Schjerling P, Wojtaszewski JF, Richter EA. Genetic impairment of {alpha}2-AMPK signaling does not reduce muscle glucose uptake during treadmill exercise in mice. Am J Physiol Endocrinol Metab 4 August 2009 [Epub ahead of print]
29. Lauritzen HPMM, Reynet C, Schjerling P, Ralston E, Thomas S, Galbo H, Ploug T. Gene gun bombardment-mediated expression and translocation of EGFP-tagged GLUT4 in skeletal muscle fibers in vivo. Pflugers Arch 2002;444:710–721
30. Lauritzen HP. Imaging of protein translocation in situ in skeletal muscle of living mice. Methods Mol Biol 2010;637:231–244
31. Ishikura S, Antonescu CN, Klip A. Documenting GLUT4 exocytosis and endocytosis in muscle cell monolayers. Curr Protoc Cell Biol 2010;Chapter 15:Unit 15.15
32. Endo M. Entry of fluorescent dyes into the sarcotubular system of the frog muscle. J Physiol 1966;185:224–238
33. Lännergren J, Bruton JD, Westerblad H. Vacuole formation in fatigued single muscle fibres from frog and mouse. J Muscle Res Cell Motil 1999;20:19–32
34. Lännergren J, Bruton JD, Westerblad H. Vacuole formation in fatigued skeletal muscle fibres from frog and mouse: effects of extracellular lactate. J Physiol 2000;526:597–611
35. Wang W, Hansen PA, Marshall BA, Holloszy JO, Mueckler M. Insulin unmasks a COOH-terminal Glut4 epitope and increases glucose transport across t-tubules in skeletal muscle. J Cell Biol 1996;135:415–430
36. Khan AH, Thurmond DC, Yang C, Ceresa BP, Sigmund CD, Pessin JE. Munc18c regulates insulin-stimulated GLUT4 translocation to the transverse tubules in skeletal muscle. J Biol Chem 2001;276:4063–4069
37. Schertzer JD, Antonescu CN, Bilan PJ, Jain S, Huang X, Liu Z, Bonen A, Klip A. A transgenic mouse model to study glucose transporter 4 myc regulation in skeletal muscle. Endocrinology 2009;150:1935–1940
38. Fazakerley DJ, Lawrence SP, Lizunov VA, Cushman SW, Holman GD. A common trafficking route for GLUT4 in cardiomyocytes in response to insulin, contraction and energy-status signalling. J Cell Sci 2009;122:727–734
39. Richter EA, Garetto LP, Goodman MN, Ruderman NB. Muscle glucose metabolism following exercise in the rat: increased sensitivity to insulin. J Clin Invest 1982;69:785–793
40. Douen AG, Ramlal T, Rastogi S, Bilan PJ, Cartee GD, Vranic M, Holloszy JO, Klip A. Exercise induces recruitment of the "insulin-responsive glucose transporter": evidence for distinct intracellular insulin- and exercise-

recruitable transporter pools in skeletal muscle. J Biol Chem 1990;265:13427–13430
41. Coderre L, Kandror KV, Vallega G, Pilch PF. Identification and characterization of an exercise-sensitive pool of glucose transporters in skeletal muscle. J Biol Chem 1995;270:27584–27588
42. Karlsson HK, Chibalin AV, Koistinen HA, Yang J, Koumanov F, Wallberg-Henriksson H, Zierath JR, Holman GD. Kinetics of GLUT4 trafficking in rat and human skeletal muscle. Diabetes 2009;58:847–854
43. Jessen N, Goodyear LJ. Contraction signaling to glucose transport in skeletal muscle. J Appl Physiol 2005;99:330–337
44. Hirshman MF, Goodyear LJ, Wardzala LJ, Horton ED, Horton ES. Identification of an intracellular pool of glucose transporters from basal and insulin-stimulated rat skeletal muscle. J Biol Chem 1990;265:987–991
45. Goodyear LJ, Hirshman MF, Horton ES. Exercise-induced translocation of skeletal muscle glucose transporters. Am J Physiol 1991;261:E795–E799